Computed and Measured Wall Interference in a Slotted Transonic Test Section

Yngve C-J. Sedin*
Saab-Scania AB, Linköping, Sweden
and
Hans Sörensén†
FFA, The Aeronautical Research Institute of Sweden, Bromma, Sweden

Attempts to computationally reconstruct observed flows about a body in a slotted transonic test section are presented, including the main features of the slot flow. The results show that viscous effects are of great importance and must be accounted for in applying the basic inviscid wall theory. Encouraging results have been obtained using a simple viscous flow model to correct for viscous effects. A number of computed cases are shown where pressure distributions and slot flow properties are compared to experimental data for an axisymmetric body in an octagonal-shaped test section provided with eight similar slots.

Nomenclature

$A(x)$ = $\ell n[a_s(x)]$, Eqs. (7-9)
$a(x)$ = geometrical slot width, Fig. 3
a_s = effective slot width
C_p = pressure coefficient, $= (p-p_\infty)/(\rho_\infty U_\infty^2/2)$
E = unit step function; $E(y)=1, y>0$; $E=0, y<0$
ℓ = slot depth, Fig. 3
m = mass flow/unit length through slot
M = Mach number
M_∞ = nominal Mach number in freestream reference flow
N = number of slots
p = pressure; pressure surface
p_p = pressure in plenum chamber
p_∞ = nominal pressure in freestream reference flow
q_s = effective slot volume flux/unit length
Q = normalized slot flow potential (see Ref. 1)
r = radius vector in cross-flow plane, normalized to $r=1$ at tunnel wall (r_w)
U = axial velocity in x direction
U_∞ = nominal velocity in freestream reference flow ($U_\infty=1$)
V = transversal cross-flow velocity, Figs. 1 and 3
v = normalized slot flow velocity (see Ref. 1)
x = coordinate along tunnel axis, Figs. 1 and 3
x_0 = slot start, upstream boundary of computational domain
x_1 = downstream end of computational domain
y,z = Cartesian coordinates at slot, Fig. 3
y_p = coordinates of line in slot centerplane where the plenum pressure is imposed, Figs. 1 and 3
γ = specific heat ratio, $=1.4$
δ = normalized plenum pressure, $(p_p-p_\infty)/(\rho_\infty U_\infty^2)$
δ^* = viscous boundary-layer displacement thickness
η = slot flow reduction factor due to viscous slot losses
ϕ = perturbation velocity potetial of "viscous" slot problem
$\bar{\phi}$ = perturbation velocity potential of approximation (filtered) problem
ψ = scaled two-dimensional harmonic slot cross-flow potential
ρ = mass density
ρ_∞ = nominal density in freestream reference flow

Subscripts

a = slot width
i = interior
p = plenum, plenum pressure surface
s = slot flow
U = axial velocity

Introduction

THE costs of tunnel testing have gone up exponentially in recent decades. At the same time, computation costs have dramatically decreased for a given flow problem. However, the time when we can rely solely upon computations still seems to be far in the future, partly due to limitations in the speed and storage capacities of present-day computers. Thus, a synthesis between wind tunnel testing and computation still is the only practical solution. This includes the use of computational methods for finding even better wind tunnel correction and operating strategies for minimizing or eliminating the wall interference.

In Ref. 1, Berndt presented an inviscid theory of wall interference in three-dimensional slotted wall test sections. His theory was the outcome of an experimental and theoretical investigation in two dimensions earlier reported on by Berndt and Sörensén.[2] In previous papers,[3-5] a number of three-dimensional pure inviscid theoretical calculations for both symmetric and asymmetric flowfields were reported by Karlsson and Sedin using the theory of Ref. 1. The present paper is a follow-up to these, but now the theory is confronted with experimental data obtained by Sörensén and Nedersjö[6] in a three-dimensional test section.

It was discovered early that larger disagreements were obtained in three dimensions than in two[2] when comparing measured and computed wall pressures using the inviscid theory. Numerical experiments and physical observations then showed that viscous effects are of paramount importance in three dimensions. The aim then was set to correct the inviscid theory in as simple a way as possible for viscous phenomena, while trying to preserve its original simplicity.

Presented as Paper 84-0243 at the AIAA 22nd Aerospace Sciences Meeting, Reno, NV, Jan. 9-12, 1984; received Feb. 25, 1984; revision received Feb. 22, 1985.

*Senior Research Scientist, Computational Aerodynamics, Aerospace Division.
†Senior Research Scientist, Head Transonic-Supersonic Section.

Phenomenological Description of Wall Theory

The wall theory of Ref. 1 is built on the calculation of an approximate interior solution filtered with respect to higher-order variations caused by the slots. To obtain the proper outer boundary conditions for the interior flow, the pressure difference between the plenum chamber and the interior has to be established in mathematical terms. The physical elements of an estimation of this pressure difference are schematically shown and titled in Figs. 1 and 2.

The pressure difference across the slot flow region can be calculated by integrating the momentum equation. Neglecting the viscous stress terms, the cross-flow part of the momentum equation in the centerplane of a slot is

$$\frac{\partial p}{\partial y} = -\rho U \frac{\partial V}{\partial x} - \frac{1}{2}\rho \frac{\partial}{\partial y} V^2 \tag{1}$$

where p is the pressure, ρ the density and U and V are the axial and transversal velocities, respectively. Now, to integrate Eq. (1) in the slot centerplane from the interior up through the slot until the plenum pressure surface is reached, the cross flowfield V must be estimated. This can be done using local small-disturbance cross-flow theory for the slots.[1,2]

To work out the two-dimensional slot cross-flow velocity potential, the transversal mass flux balance has to be considered. This is in order to define the flux through each slot. The flux balance is schematically illustrated in Fig. 2. The slot flux per unit length is made up by the flux coming from the interior and from the wall boundary layer. Once the slot fluxes are known, the corresponding incompressible cross-flow solution makes it possible to estimate the pressure difference $(p_p - p_i)$ between the plenum pressure surface and the interior flow. This was done in Ref. 1 using a matched asymptotic expansion in which the outer boundary of the interior flow was extended to the wall. Thus, when the plenum pressure p_p is known, the interior pressure p_i can be determined to serve as a boundary condition. The slot fluxes are a priori unknown and must be solved together with the interior flow in an iterative manner.

At first, considerable discrepancies were encountered when comparing pure inviscid wall pressure calculations to experimental data. This called for the inviscid theory to be corrected for viscous effects. Figure 3 indicates some effects that may be of importance to a corrected theory. In the slot centerplane, due to the viscosity, the axial velocity U is varying like a shear flow profile, causing losses of axial momentum. The cross-flow velocity V is varying like a boundary-layer profile within the slot, giving an increased core velocity for a given mass flux. Another situation obtains when the flow is separating at the slot inlet corners, forming rolled up vortex sheets. An increased core velocity V is then also likely to appear due to the partly blocked slot width.

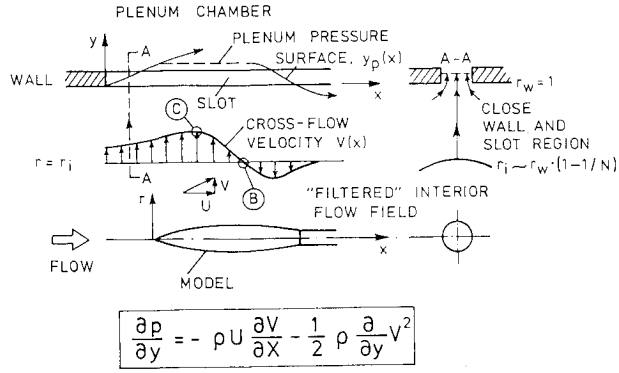

Fig. 1 Integration of momentum equation from the interior to the plenum pressure surface.

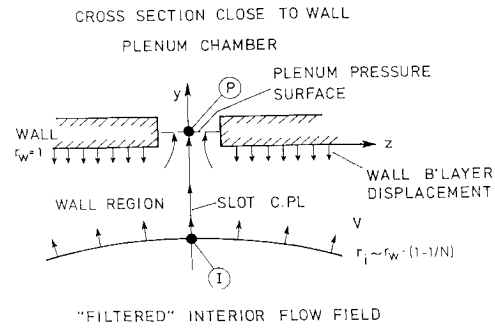

Fig. 2 Cross-flow mass flux balance and pressure integration path (I-P).

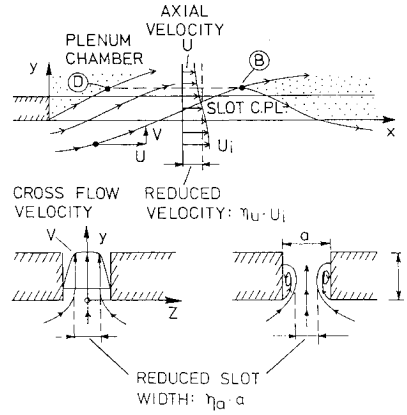

Fig. 3 Reduced slot width and axial velocity to correct for viscous effects.

Inviscid Theory Corrected for Viscous Effects: Symmetric Flows

Now, following the ideas of Refs. 1 and 2, Eq. (1) should be integrated in the centerplane of each slot to obtain the boundary conditions for the interior. To do so, the velocities U and V must have "representative values" with regard to viscous effects within the slot region. The previous discussion of Fig. 3 suggests that this can be achieved by using reduced values for the axial velocity and the slot width. In reality, these reductions are likely to vary along the centerplane. However, to keep the overall simplicity of the physical and mathematical model, the simplest possible correction will be adopted. That is, to use constant reduction effectiveness factors η_U, η_a everywhere (see Fig. 3).

The first term on the right-hand side of Eq. (1) dominates when $V \approx 0$, while the second term is important when $V_x \approx 0$. These two distinguished limits, located at x stations corresponding to points B and C in Fig. 1, will be important for the choice of the reduction factors, η_a for the slot width and η_U for the axial velocity. Thus, these two factors are chosen by matching the computed wall pressures to experimentally observed pressures at these distinguished x stations. In this way, experimentally obtained data are computationally reconstructed and can be compared at all other points. This will be done computationally by using the measured quiescent plenum pressure.

In inviscid small-disturbance theory, the coefficients ρU and ρ of the terms on the right-hand side of Eq. (1) are set to freestream reference flow values, $\rho_\infty U_\infty$ and ρ_∞, respectively. In the present viscous theory, they will be substituted by representative slot flow values $\rho_s U_s$ and ρ_s depending on x only.

The representative slot flow velocity U_s is assumed to be equal to the interior velocity U_i multiplied by a viscous correction factor η_U. Assuming constant total enthalpy and pressure

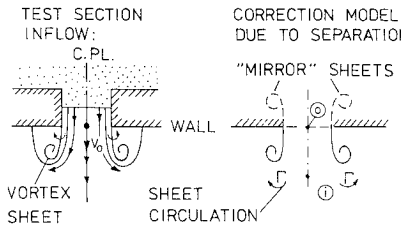

Fig. 4 Postulated test section inflow model.

then provides an estimate of a representative slot flow density ρ_s in terms of interior data, so that

$$\frac{\rho_s}{\rho_i}=\left[1+\frac{\gamma-1}{2}M_i^2(1-\eta_U^2)\right]^{-1}, \quad \frac{U_s}{U_i}=\eta_U \tag{2}$$

For axisymmetric flows, the mass flux m per unit length through each slot is approximately

$$m=2\pi\rho_i(V_i+\delta_x^*\cdot U_i)/N \tag{3}$$

where $V_i=U_\infty\bar{\phi}_r$ and $U_i=U_\infty\cdot(1+\bar{\phi}_x)$ are taken at the wall. Here δ^* is the wall boundary-layer displacement thickness and N the number of slots, while $\bar{\phi}$ is the symmetric small-disturbance potential of the interior "filtered" flow problem. We now write the "composite" perturbation potential ϕ in the "viscous" slot flow region in the form

$$\phi=\bar{\phi}(x,1)+(U_s/U_\infty)\cdot\Psi(y,z;x) \tag{4}$$

where Ψ is a harmonic two-dimensional cross-flow potential function based on velocity U_s. The outer expansion of Ψ is zero at $y=-1/N$, $z=0$. Close to and within the slot Ψ_y has its largest values. With this in mind and inserting $V=U_\infty\cdot\phi_y$ into Eq. (1), the pressure difference across the viscous slot flow region can be approximately integrated in the plane $z=0$ from $y=-1/N$ to $y=y_p(x)$ as

$$\delta+\bar{\phi}_x(x,1)=-\left(\frac{\rho_s}{\rho_\infty}\right)\cdot\left(\frac{U_s}{U_\infty}\right)\left(\frac{\partial}{\partial x}\left[\left(\frac{U_s}{U_\infty}\right)\Psi\right]\right)_p$$

$$-\frac{1}{2}\left(\frac{\rho_s}{\rho_\infty}\right)\cdot\left(\frac{U_s}{U_\infty}\right)^2[(\Psi_y)^2]_p \tag{5}$$

where subscript p indicates values along the plenum pressure surface $y_p(x)$. The parameter δ is the normalized plenum pressure coefficient. Thus, Eq. (5) constitutes the outer boundary condition for the symmetric inviscid interior flow to be applied at the wall ($r_w=1$).

To determine Ψ, the slot volume flux and the plenum pressure surface position are required. Recalling that Ψ is based on U_s and combining Eq. (3) with a simplified mass flux balance within the slot, the following effective slot flux and slot width variables result:

$$q_s=m/(\rho_s\cdot U_s), \quad a_s=\eta_a\cdot a \tag{6}$$

where a denotes the original geometrical slot width, while η_a is the reduction factor due to viscous effects and m is given by Eq. (3). The equation for the plenum pressure surface $y_p(x)$ (outside the "jet region" D-B of Fig. 3) then is

$$\frac{dy_p}{dx}=q_s\frac{v}{a_s}-\frac{dA}{dx}\cdot y_p\cdot E \tag{7}$$

In the "jet region" D-B (Fig. 3), the position of $y_p(x)$ is as defined in Ref. 1. $v(y_p/a_s)$ is a normalized velocity slot flow function and $E(y_p)$ the unit step function active inside slot. The variable A denotes $A=\ell n a_s$. Now, following Refs. 1 and 4, Ψ can be written down for the axisymmetric case with N uniformly distributed slots in a cylindrical test section,

$$\Psi(y,0;x)=q_sQ-\frac{q_s\cdot[\ell n(N)+A]}{\pi}-y^2\cdot\frac{dA}{dx}\cdot\frac{E}{2} \tag{8}$$

$Q(y/a_s)$ is a normalized slot flow velocity potential function that, together with $v(y/a_s)$, can be found in Refs. 1 and 4. The cross-flow velocity V in the plane $z=0$ then is $U_s\cdot\Psi_y$, where Ψ_y is

$$\Psi_y=q_s\frac{v}{a_s}-\frac{dA}{dx}\cdot y\cdot E \tag{9}$$

To close the equations, the functions ρ_s/ρ_∞ and U_s/U_∞ of Eq. (5) must be given. By use of Eq. (2), these functions will be

$$\frac{\rho_s}{\rho_\infty}=\frac{1-M_\infty^2\bar{\phi}_x(x,1)}{1+[(\gamma-1)/2]M_i^2(1-\eta_U^2)}, \quad \frac{U_s}{U_\infty}=[1+\bar{\phi}_x(x,1)]\eta_U \tag{10}$$

where $M_i(x)$ is the "interior" Mach number at $r_w=1$ and $\bar{\phi}_x(x,1)$ the interior disturbance velocity. In Eq. (10) ρ_i and M_i have been approximated by

$$\rho_i/\rho_\infty=1-M_\infty^2\cdot\bar{\phi}_x(x,1), \quad M_i=M_\infty[1+(\gamma+1)\bar{\phi}_x(x,1)]^{1/2} \tag{11}$$

In summary, the features of the revised theory are analogous to the original inviscid theory of Ref. 1. Equations (5-8) have the same type of structure and they transform into each other when the representative slot flow values (ρ_s, U_s) and the interior density ρ_i are set to freestream reference values. Integration of Eq. (5) yields an outer Dirichlet boundary condition at $r=1$ to the filtered problem in terms of the slot fluxes. The numerical integration of Eq. (5) develops in much the same way as was reported in Ref. 4.

Field Equation and Boundary Conditions

The field equation to be solved between the model and the wall is the axisymmetric small-perturbation equation

$$[1-M_\infty^2-M_\infty^2(\gamma+1)\bar{\phi}_x]\bar{\phi}_{xx}+(r\bar{\phi}_r)_r/r=0 \tag{12}$$

The potential $\bar{\phi}$ is the filtered solution close or equal to the "exact" solution in the neighborhood of the axisymmetric model. M_∞ is the freestream Mach number of the chosen reference flow. Equation (12) is solved numerically using the finite difference method of Ref. 7. As an upstream inflow condition at $x=x_0$, $\bar{\phi}=0$ is given, while at the downstream outflow section ($x=x_1$), $\bar{\phi}_{xx}=0$ is assumed. The outer boundary condition at the wall ($r=1$) is found by integration of Eq. (5). The iterative procedure for solving the nonlinear system of equations [Eqs. (5-8) and (12)] is as outlined in Ref. 4.

To account for the turbulent wall boundary layers, a two-dimensional layer is calculated on the test section wall halfway between the slots. On the body surface, an axisymmetric boundary-layer equation is applied, whereupon the displacement thickness is added on top of the body radius forming the slender-body condition at $r=0$. The boundary-layer displacement thickness equations are based on the integral momentum equation.

Additional Comments on the Slot Flow Model

Early numerical calculations using the revised slot flow model indicated shock wave positions slightly upstream, at the wall as well as the body, as compared to experimental measurements. This was in spite of the conservative numerical scheme being used.

One reason for this might be that a vortex sheet separation also occurs at the slot corners when the flow is coming back into the test section.[1] This would essentially inflict upon the

streamline curvature term of Eq. (1) when integrated. To see qualitatively the influence of such a flow, a corrected flow model was postulated as shown in Fig. 4. Using a convective time model in the cross-flow planes, it was possible to qualitatively estimate the growth of circulation $\Gamma(x)$ within the separated vortex sheets. When a no-slip condition was imposed on the slot sides, the growth of circulation Γ within each sheet then came out to be

$$\frac{d\Gamma}{dx} = \frac{1}{2}\frac{U_s}{U_\infty}\cdot\left(\frac{V_0}{U_s}\right)^2 \cdot E(y_p) \tag{13}$$

where $V_0 < 0$ is the velocity at the slot entrance and E the unit step function. V_0 is effectively set by the cross-flow mass flux equation. Hence, the correction term to the cross-flow potential ϕ at the plenum surface $y_p(x)$ is found by integrating $-d\Gamma/dx$ from Eq. (13).

The x integration of Eq. (13) starts at the flow reversal point, see Fig. 3. It is interesting to note that the correction term approximately will cancel the quadratic cross-flow term on the right-hand side of Eq. (5) and hence probably move the shock slightly downstream. This expected action was verified by calculations.

Experimental Setup and Instrumentation

The experiments were carried out in a tunnel at the Aeronautical Research Institute of Sweden (FFA). The tunnel is a closed-circuit, continuous tunnel with an octagonal test section of 0.7 m^2, with slots in the corners. The ventilation is 9.2% of the total periphery at the model location. The test section with model and slot is shown in Figs. 5 and 6. The instrumentation setup is shown in Fig. 6.

The size of the parabolic arc body gave a blockage ratio of 2.23%. The Reynolds number was roughly 10^7, based on the body length (0.996 m). The body fineness ratio was $6\cdot\sqrt{2}$. The reason for using a very big model was to ensure a strong cross flow within the slots.

To see the influence of slot depth, one shallow (19 mm) and one deep (52 mm) slot were tested. The depth is important when integrating the streamline curvature term of Eq. (1) through the slot.

Some Slot Flow Measurements

Figure 7 illustrates flow inclinations within the deep slot ($\ell = 52$ mm) as obtained by oilflow visualizations at Mach number 0.98. The flow angles were measured by hand on different photographs. Interpretation difficulties and different camera angles imply the data scattering. The upper part of Fig. 7 shows the transversal core velocity in the slot centerplane just at the slot entrance ($y = 0$, $z = 0$).

The lower part of Fig. 7 shows the cross-flow inclination at the slot sidewall just inside the slot entrance corner ($y = +0$, $z = a/2$). Here, it is interesting to see how the center core velocity (inclination) and the slot side wall cross-flow velocity roughly agree from the slot start up to about $x = 600$ mm. After that x station, the slot side wall inclination rapidly falls off and indicates a flow reversal after $x = 800$, while the center core cross-flow velocity there still indicates a main in-

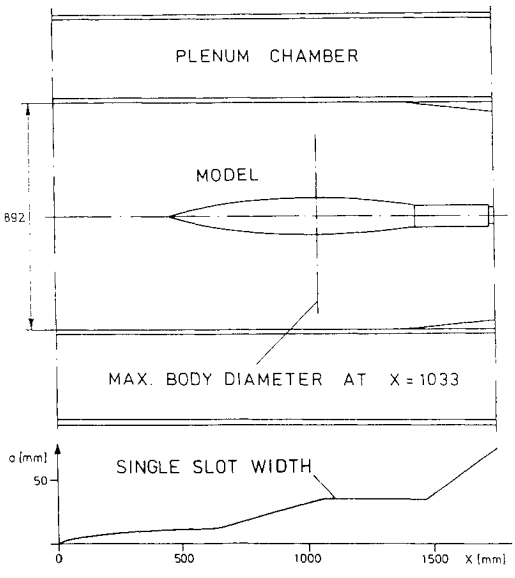

Fig. 5 Test section with model and slot width.

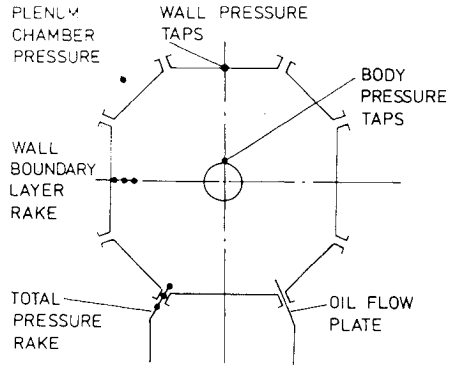

Fig. 6 Test section instrumentation.

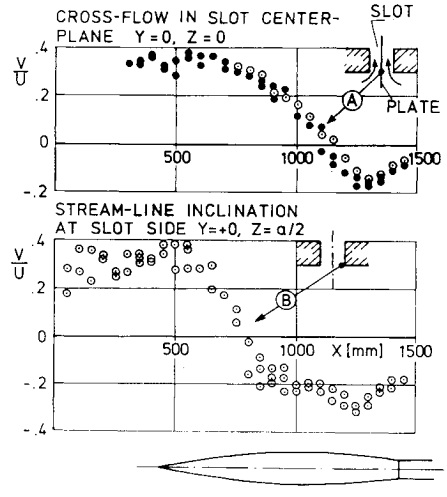

Fig. 7 Slot flow streamline inclinations by oilflow visualizations, deep slot, $M_\infty = 0.98$.

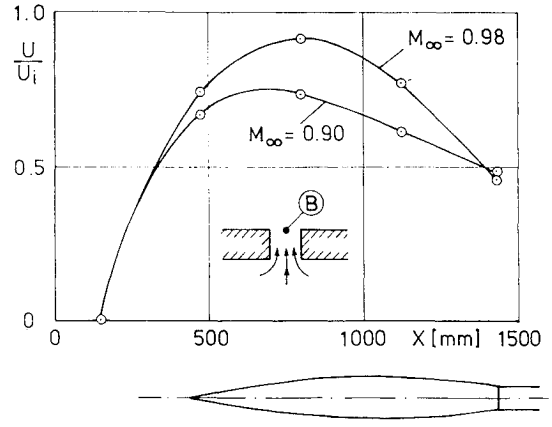

Fig. 8 Mach number effects on axial velocity measured close to slot exit, deep slot.

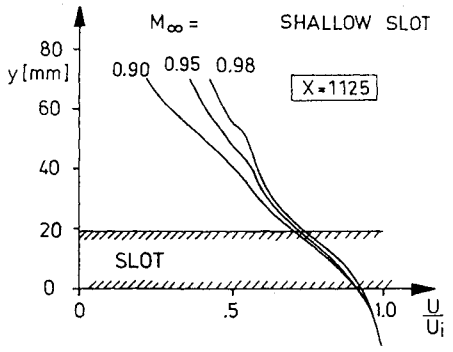

Fig. 9 Measured velocity profiles in slot centerplane, shallow slot.

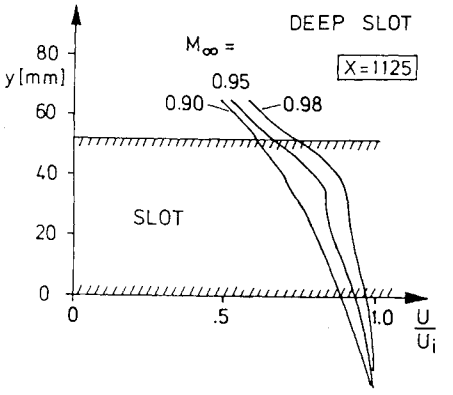

Fig. 10 Measured velocity profiles in slot centerplane, deep slot.

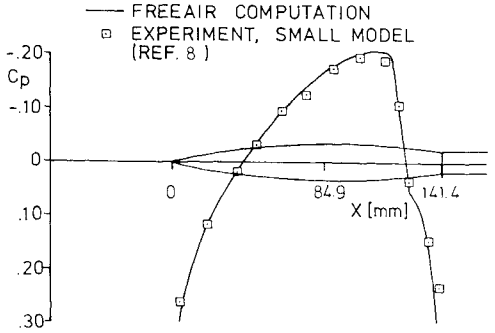

Fig. 11 Freeair computation check of finite-difference procedure at $M_\infty = 0.98$.

flow into the slot. It is not until about $x = 1100$ that the main center core stream indicates a flow reversal into the test section again. This behavior seems to indicate that a vortex flow separation is starting at the slot inlet corners around $x = 600$ and continues after that. Moreover, reminiscences of this axial vorticity with its original direction of circulation still seem to persist within the slot even downstream of $x = 1100$, where the main center core flow returns into the test section.

Figures 8-10 show Mach number effects on the axial velocity within and outside the slot. The measurements were taken in the slot centerplane. Comparing Figs. 9 and 10, it is obvious that the deep slot is more affected by viscosity and by Mach number variations than the shallow one. The Mach variations as such are consistent in the meaning that lower Mach numbers imply larger velocity losses for both slots. This probably is a result of the fact that lower Mach numbers are producing smaller cross-flow velocities within the slots, giving the test section wall boundary layer an opportunity to contaminate the slot center core flow. Right above the model, the

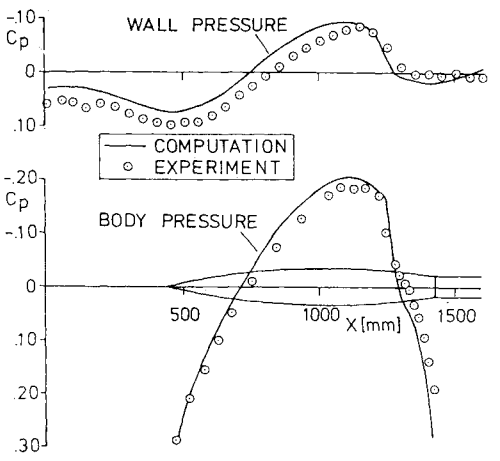

Fig. 12 Computation without viscous slot flow losses, shallow slot, $M_\infty = 0.98$.

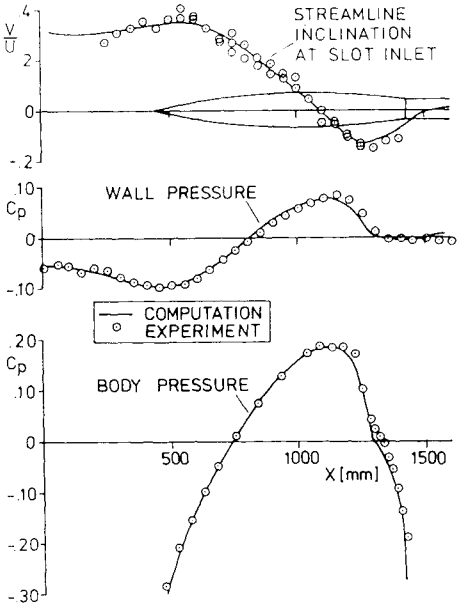

Fig. 13 Computation with viscous slot flow losses, shallow slot, $M_\infty = 0.98$.

Table 1 Data for calculated cases

Fig.	M_∞	δ	η_a	η_U	Slot
12	0.982	−0.0066	1.00	1.00	Shallow
13	0.982	−0.0066	0.77	0.75	Shallow
14	0.900	−0.0072	0.77	0.75	Shallow
15	0.982	−0.0058	0.71	0.69	Deep
16	0.898	−0.0076	0.55	0.54	Deep

ratio between the wall boundary layer thickness and the slot width is about 0.6.

Numerical Computations

Figures 11 and 12, belonging to an introductory phase, give a perspective on how well the finite difference method captures a real, almost interference free flow (see Fig. 11) as well as an illustration to the failure of the purely inviscid slot flow model (see Fig. 12).

Figures 13-16 are devoted to the objective of computationally reconstructing observed pressure distributions in the tun-

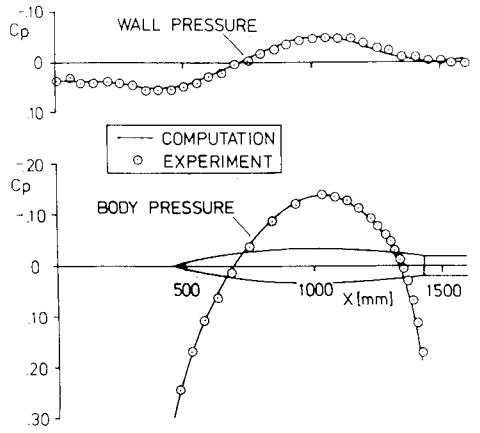

Fig. 14 Computation with viscous slot flow losses, shallow slot, $M_\infty = 0.90$.

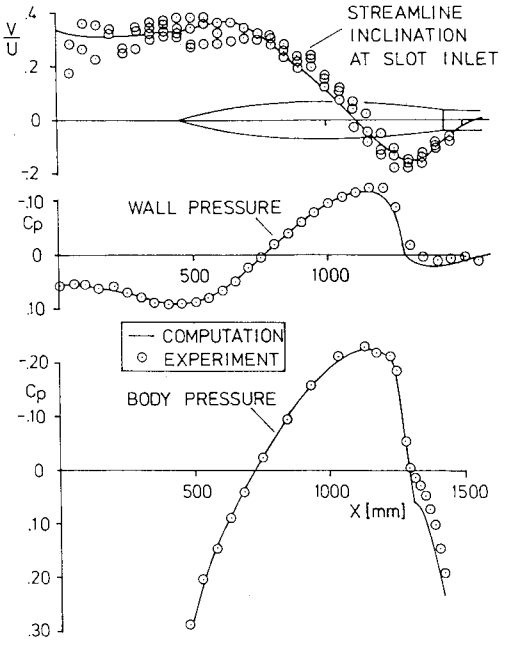

Fig. 15 Computation with viscous slot flow losses, deep slot, $M_\infty = 0.98$.

nel using the outlined wall theory. Input data for these calculations are shown in Table 1. M_∞ denotes the nominal freestream reference Mach number that "labels" the tunnel calibration data; δ, which is a part of the tunnel setting, is the measured normalized plenum pressure coefficient; η_a and η_U are viscous reduction factors for the slot width and the axial slot flow velocity.

The numerical computations were conducted by applying the test section inflow model sketched in Fig. 4. The values of η_a and η_U were found iteratively by perturbation analysis of the streamline curvature and the cross-flow terms of Eq. (1) with respect to η_a and η_U. This was done in order to simultaneously force computed C_p values in two points on the wall to agree with measured data at x stations corresponding to points B and C of Fig. 1. This problem is nonlinear, so it has to be solved by iteration. Because the shallow slot seemed to be affected to only a minor degree by the Mach number (see Fig. 9), the values of η_U and η_a were kept constant for all Mach numbers in this case. These values for the shallow slot were evaluated at $M_\infty = 0.982$. For the deep slot, the Mach number effects (see Fig. 10) were not negligible. Hence, individual values depending on the Mach number were necessary.

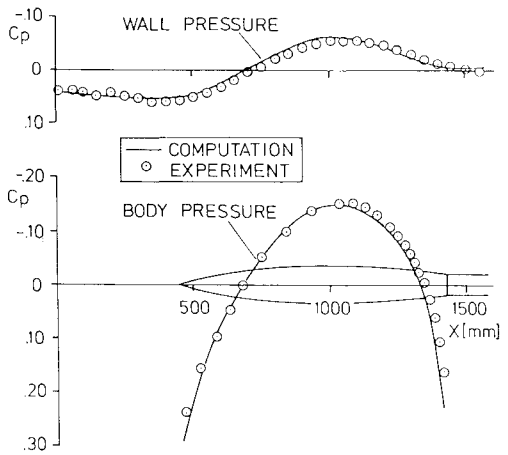

Fig. 16 Computation with viscous slot flow losses, deep slot, $M_\infty = 0.90$.

The finite difference grid was uniform in the streamwise direction and nonuniform in the radial. The number of mesh points was 63×65 in x and r directions, respectively, 31 x points covering the length of the body. The test section was approximated by a circular cylinder and the slots were uniformly distributed over the wall. Running times on a VAX 11/782 computer were in the range of 30-45 CPU min depending on the Mach number. However, a cut by one-third of the running time is probably within reach. The iterations were stopped when the maximum potential correction was less than 10^{-6}.

Comments on the Numerical Results

Figure 11 shows how the finite difference method is able to capture a real "interference-free" flow quite well. The agreement between the free air computed pressure distribution and the experimental data from Ref. 8 is very good for this high Mach number ($M_\infty = 0.98$). The experiments were performed with a model blockage ratio of 0.15%. The calculations were conducted by applying the freestream reference pressure at 6.3 body lengths outside the body.

Figure 12 clearly illustrates the inadequacy of the original inviscid wall theory at $M_\infty = 0.98$, when no slot flow losses were considered.

A dramatic improvement is found in Fig. 13 when the viscous slot flow corrections are incorporated. Furthermore, it is interesting to see how the value of η_U (Table 1) is close to what can be read from Fig. 9 just at the slot exit for Mach number 0.98 at $x = 1125$, which is close to $x = 1100$, where the flow reversal takes place within the slot. Moreover, in Fig. 13, a surprisingly good agreement is found between computed and measured streamline inclination angles at $y = 0$, $z = 0$. This further confirms the theory.

Figure 14 shows calculations concerning the shallow slot at Mach number 0.90. In these computations, the slot flow losses were kept the same as for Mach number 0.98 (Fig. 13). Generally, there seems to be a minor upstream shift of the pressure signature on the wall in the calculations. This also manifests itself in a slightly too strong recompression on the aft part of the body. This seems to be true even for Mach number 0.98 (Fig. 13). One reason for this might be that locally a lower plenum pressure than presently used should be applied along the separating streamline after flow reversal has occurred within the slot.

Figures 15 and 16 show calculations with the deep slot. The deep slot characterizes itself by keeping up a larger pressure difference between the wall and the plenum chamber than was the case with the shallow slot (compare Figs. 13 and 15). The reason for this is that the streamline curvature term of Eq. (1)

is integrated over a larger slot depth, which most strongly affects the results at about $x = 1100$ where the cross-flow velocity is zero. In general terms, the agreement with experiments is also comparatively good for this slot depth. Due to Mach numbers effects (see Figs. 8 and 10), it was deemed necessary to evaluate individual slot flow losses for Mach numbers 0.98 and 0.90. These η_U values can also be read from Fig. 10 just outside the slot exit on the plenum side. Thus, a rule of thumb seems to be that representative values of η_U can be found from experimental data close to the slot exit at that location where the flow reversal takes place within the slot.

Looking at the details of Figs. 15 and 16 (concerning the deep slot), the recompression over the aft part of the body here is also a bit too strong in the calculations. Thus, the previous discussion about the plenum pressure might be applicable here as well. Concerning the Mach number 0.98 case (Fig. 15), a shock/boundary-layer interaction ramp has been tried for both the body and wall. This improved the computed results in the recompression region, but moved the shock upstream. However, it is likely that the shock would move downstream again if a lower plenum pressure was then applied behind the flow reversal point.

Conclusions

Summing up so far the continuing FFA/SAAB investigation of slotted wall flow,[9] there seems to be good hope for a reasonable agreement between experiments and computations if viscous effects are qualitatively modeled and implemented within the inviscid theory. Thus, the corrected inviscid theory can be a viable tool for wind tunnel testing in the search for improved operational strategies for slotted wall tunnels with a reasonable amount of computational efforts involved. This is because the numerical model is simple enough for repeated use.

What remains for the future is to adapt the method to test sections of arbitrary shapes and three-dimensional flows. Steps in that direction have been taken[10] using a local slot boundary condition rather than a homogenous one, but with the present slot flow model.

References

[1]Berndt, S.B., "Inviscid Theory of Wall Interference in Slotted Test Sections," *AIAA Journal*, Vol. 15, Sept. 1977, pp. 1278-1287.

[2]Berndt, S.B. and Sörensén, H., "Flow Properties of Slotted Walls for Transonic Test Sections," AGARD CP 174, 1975.

[3]Karlsson, K.R. and Sedin, Y.C-J., "Axisymmetric Calculations of Transonic Wind Tunnel Interference in Slotted Test Sections," *AIAA Journal*, Vol. 17, Aug. 1979, pp. 917-919.

[4]Karlsson, K.R. and Sedin, Y.C-J., "Numerical Design and Analysis of Optimal Slot Shapes for Transonic Test Sections—Axisymmetric Flows," *Journal of Aircraft*, Vol. 18, March 1981, pp. 168-175.

[5]Sedin, Y.C-J. and Karlsson, K.R., "Some Theoretical Wall-Interference Calculations in Slotted Transonic Test Sections—Three Dimensional Flows," *Proceedings of the 13th Congress of the International Council of the Aeronautical Sciences*, Seattle, WA, Vol. 1, Aug. 1982.

[6]Sörensén, H. and Nedersjö, S.E., "Wall-Interference Measurements of Large Models and Different Slot Depths," unpublished work done at FFA (The Aeronautical Research Institute of Sweden), Nov. 1980.

[7]Sedin, Y.C-J., "Axisymmetric Sonic Flow Computed by a Numerical Method Applied to Slender Bodies," *AIAA Journal*, Vol. 13, April 1975, pp. 504-511.

[8]Drougge, G., "An Experimental Investigation of the Interference Between Bodies of Revolution at Transonic Speeds with Special Reference to the Sonic and Supersonic Area Rules," FFA, Stockholm, Rept. 83, 1959.

[9]Berndt, S.B., "Flow Properties of Slotted-Wall Test Sections," *Wall Interference in Wind Tunnels*, AGARD CP 335, 1982, pp. 6-1-6-7.

[10]Sedin, Y.C-J. Agrell, N., and Zhang, N., "A Local Slot Boundary Condition for Transonic Flow Calculations in Slotted-Wall Test Sections of Wind Tunnels," FFA, Stockholm, Rept. TN 1984-34, 1984.